Simulation framework to estimate the performance of CO_2 and O_2 sensing from space and airborne platforms for the ASCENDS mission requirements analysis

Denis Pliutau, and Narasimha S. Prasad *

NASA Langley Research Center, 5 N. Dryden St., MS 468, Hampton VA, 23681

ABSTRACT

The Active Sensing of CO_2 Emissions over Nights Days and Seasons (ASCENDS) mission recommended by the NRC Decadal Survey has a desired accuracy of 0.3% in carbon dioxide mixing ratio (XCO2) retrievals requiring careful selection and optimization of the instrument parameters. NASA Langley Research Center (LaRC) is investigating 1.57 micron carbon dioxide as well as the 1.26-1.27 micron oxygen bands for our proposed ASCENDS mission requirements investigation. Simulation studies are underway for these bands to select optimum instrument parameters. The simulations are based on a multi-wavelength lidar modeling framework being developed at NASA LaRC to predict the performance of CO_2 and O_2 sensing from space and airborne platforms. The modeling framework consists of a lidar simulation module and a line-by-line calculation component with interchangeable lineshape routines to test the performance of alternative lineshape models in the simulations. As an option the line-by-line radiative transfer model (LBLRTM) program may also be used for line-by-line calculations. The modeling framework is being used to perform error analysis, establish optimum measurement wavelengths as well as to identify the best lineshape models to be used in CO_2 and O_2 retrievals. Several additional programs for HITRAN database management and related simulations are planned to be included in the framework. The description of the modeling framework with selected results of the simulation studies for CO_2 and O_2 sensing is presented in this paper.

1. INTRODUCTION

The Active Sensing of CO_2 Emissions over Nights Days and Seasons (ASCENDS) mission aimed at global measurement of the carbon dioxide mixing ratio (XCO_2) using active sensing approach is being investigated by a number of groups [1]. Several measurement approaches in alternative bands of CO_2 and O_2 are being evaluated for potential implementation by different NASA centers including LaRC, GSFC (Goddard), and JPL. The retrieval of the XCO_2 with the desired accuracy of ~ 0.3% places very strict constraints on the lidar system parameters and requires ingenious selection of the retrieval approaches to minimize errors.

In order to evaluate the lidar system requirements and aid in selecting optimum excitation wavelengths and methodology, we have developed a multi-wavelength lidar modeling framework for space or airborne lidar simulations. The modeling framework is used for comparative analysis of alternative measurement approaches for the sensing of CO_2 and O_2. The analysis includes general lidar sensitivity, effects of laser stability as well as the perceived requirements on the weighting functions. The framework also includes additional programs and extends the usability of the modeling package beyond the scopes of the ASCENDS mission to the analysis of other molecules in variable spectral regions which is useful for future applications and in adjacent scientific fields. In this paper, a description of the lidar modeling framework and selected sample calculation results are presented.

2. MODELING FRAMEWORK OVERVIEW

The modeling framework consists of several programs as shown in Fig. 1. The main multi-wavelength lidar simulation program (1) which relies on the use of atmospheric transmission calculations using the LBLRTM (2), or the custom line-by-line routines (3), a program for the HITRAN database management (4), and a custom compilation of the 3D atmospheric concentrations (5) for atmospheric molecules [2-4].

The framework relies on several satellite datasets, models and 3rd party libraries as shown in Fig. 2. As can be seen, the atmospheric model profiles are based on several independent sources such as MERRA, Carbontracker, standard atmospheres, the radiosonde data, and the 3D concentration profiles for other molecules. Other datasets used in the model include the ASTER-GDEM elevation model, MODIS BRDF-adjusted surface reflectance, and optional use of CALIPSO aerosols attenuation [5-9]. Several third party open-source libraries are used for datasets handling and visualization as shown in Fig. 2 [10-12].

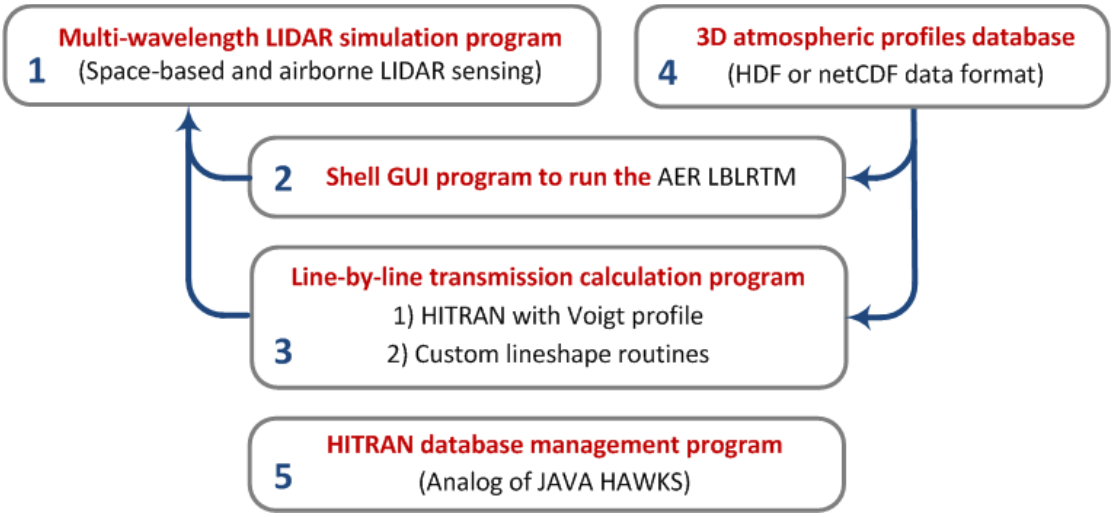

Fig. 1 Overview of the programs comprising the lidar modeling framework

While the framework involves both the standard lidar sensitivity as well as the spectroscopy related analysis, more emphasis is placed on the error factors and optimizations related to the selection of excitation wavelengths and weighting functions determined by the atmospheric transmission features variable with the atmospheric parameters.

3. LIDAR SIMULATION DESCRIPTION

3.1 General overview of the lidar framework functionality

The general overview of the framework functionality and components is presented in Fig. 3. As can be seen, several satellite datasets are used in the framework to determine atmospheric and surface parameters specific to the selected location and date/time points. The data extracted from these datasets is further processed for subsequent lidar, and transmission calculations using the AER LBLRTM and custom lidar and spectral calculation routines. The output of the simulations is a combination of lidar and spectroscopy related error estimates such as the lidar system requirements, weighting functions analysis, laser wavelength constrain requirements, and the information on excitation wavelength optimization.

Our modeling approach is based on the goal to merge the lidar simulation and transmission calculations together by using the location and date/time specific physical parameters of the atmosphere and the earth surface available from a variety of satellite observations and data assimilations. This approach effectively brings together the standard lidar sensitivity calculations with the spectroscopy aspects of the Integrated Path Differential Absorption (IPDA) approach (such as the effects of the laser wavelength stability and the weighting functions analysis and error estimate).

The previous studies only involved the lidar sensitivity analysis based on location and date/time specific databases without thorough spectroscopy related error estimates or weighting functions analysis, or only used the six available standard atmospheric models from 1976 for subsequent weighting function and laser jitter calculations [13-18]. Our simulation represents a merge of these two approaches, which in addition to the lidar sensitivity studies, brings in the capability of establishing the limitations imposed by the laser wavelength stability constraints and the chosen locations of the measurement wavelengths on the shape and errors in the resulting retrieved optical depths and the weighting functions.

The 3D atmospheric model database we are compiling for molecules other than CO_2 and O_2 is meant to be used as an alternative to the usage of the US Standard atmospheric models with the atmospheric parameters extracted on the basis of the surface coordinates, and the date and time positions.

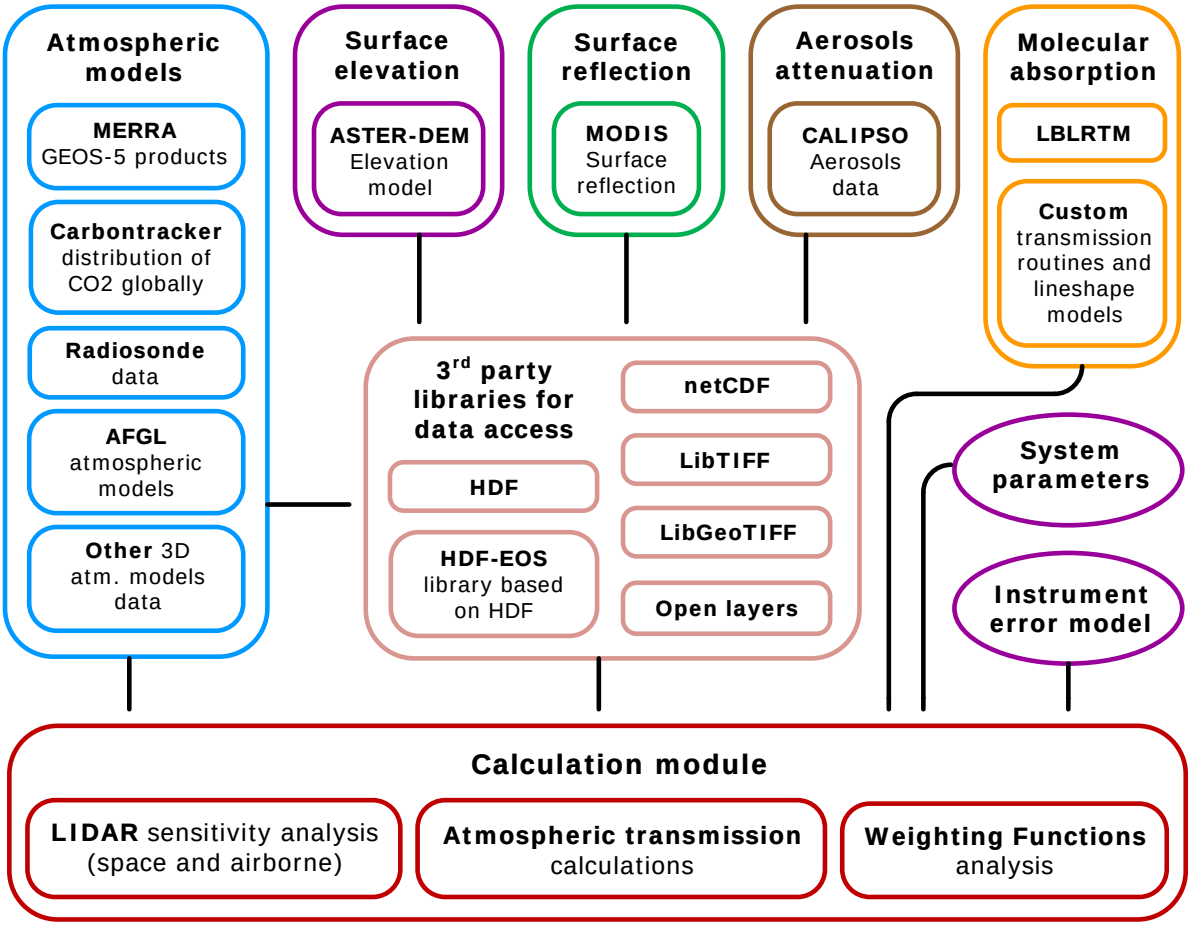

Fig. 2 Lidar modeling framework databases, components and 3rd party libraries used.

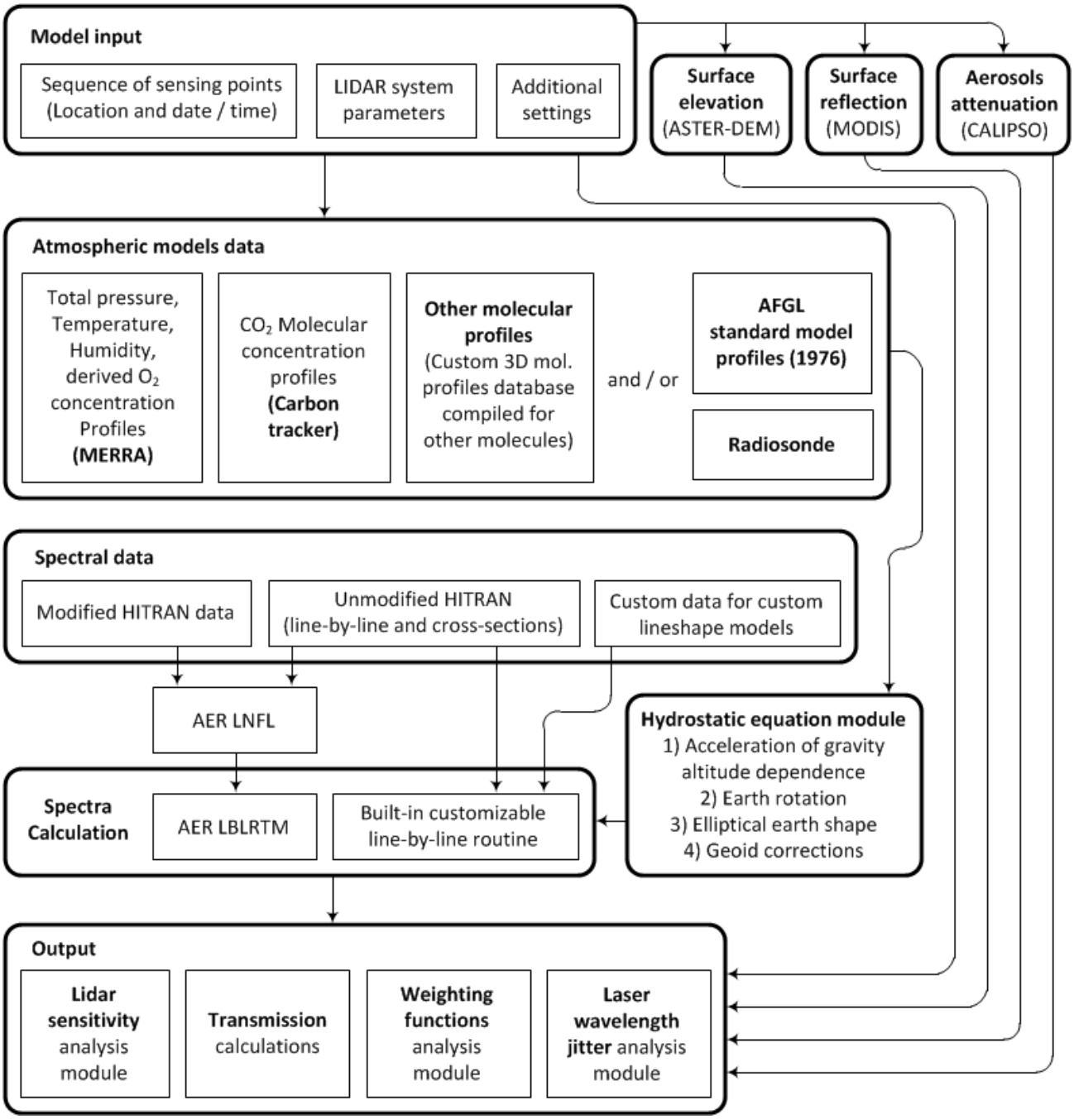

Fig. 3 General overview of the lidar framework functionality

3.2 Atmospheric models

The global atmospheric models used as input into the line-by-line calculations in this framework are derived from several different datasets obtained from independent observations, assimilations and/or models. Total pressure, temperature, and humidity are obtained from the MERRA data products [6]. Several alternative MERRA data products may be used such as the analyzed fields on model layers (inst6_3d_ana_Nv), the analyzed fields at pressure levels (inst6_3d_ana_Np), or the basic assimilated fields from IAU corrector (inst3_3d_asm_Cp). These data products are also used to derive the O_2 concentrations taking into account its proportionality to the total pressure. The concentration of CO_2 is obtained from the NOAA Carbontracker 3D mole fraction datasets [5]. These datasets are subjected to further extraction of location and date / time specific atmospheric profiles of total pressure, temperature, humidity, O_2 and CO_2 concentrations to be used for subsequent line-by-line or cross-sectional calculations.

MERRA data is used in combination with the hydrostatic equation and surface elevation values to convert pressure levels into corresponding altitude levels. This conversion also takes into account higher order errors due to the altitude dependence of the acceleration of gravity, earth rotation, as well as the earth ellipsoid with geoid corrections as described in further sections.

An important parameter affecting the precision of the line-by-line calculations is the selection of the maximum altitude cutoff value affecting the residual optical depth error. The significance of this contribution depends on the locations of the laser wavelengths selected for the on/off line measurements. For example, Fig 4 shows a comparison of the relative error due to different maximum altitude cut-off values selected for line-by-line calculations in the 1.57 micron band of CO_2 using the LBLRTM program. Spectrum 4(a) is the total optical depth calculation for a vertical path length of 100km, while (b), (c), and (d) indicate the residual relative optical depth error due to the different choice of the vertical cutoff altitude. Spectrum 4(b) corresponds to the altitude cutoff of 48km representing the maximum altitude of the Chemistry model previously used for the lidar simulations performed by Kawa et. al [13, 19]. As can be seen, such cutoff altitude results in the residual error reaching as high as 0.8% at selected wavelengths.

This difference is further illustrated in Fig.5 where the 6359.9674 cm^{-1} line of CO_2 investigated by the Goddard group is shown. As can be seen, spectrum 5(a) is the total optical depth for this selected line and spectra 5(b) and (c) show the difference between two calculations with cutoff altitudes of 100 and 48km. As can be seen, an error in excess of 0.1% in optical depth is observed within 2pm from the line center at the selected cutoff of 48km. Since the optical depth values are in direct proportionality with the gas concentration, a higher cutoff altitude must be selected to eliminate this additional uncertainty. As can be seen from Fig 4(d), an altitude of 80km proves to be sufficient to make this contribution negligible. For our simulations we have selected the datasets which conform to these requirements: the NOAA Carbontracker 3D mole fractions data is provided up to an altitude of ~80 km, and the MERRA data products are defined up to the pressure levels of 0.1 or 0.01 hPa corresponding to an altitude of ~ 80km or higher.

As an additional illustration of the cutoff altitude selection effect, Fig 6 shows a comparison of calculations for cutoff altitudes of 100km and 18km performed for a different CO_2 line. The altitude of 18km roughly corresponds to the GlobalHawk maximum flight altitude. As can be seen, errors reaching as much as 30 % are observed. Similar results were obtained for other CO_2 and O_2 lines being evaluated for ASCENDS.

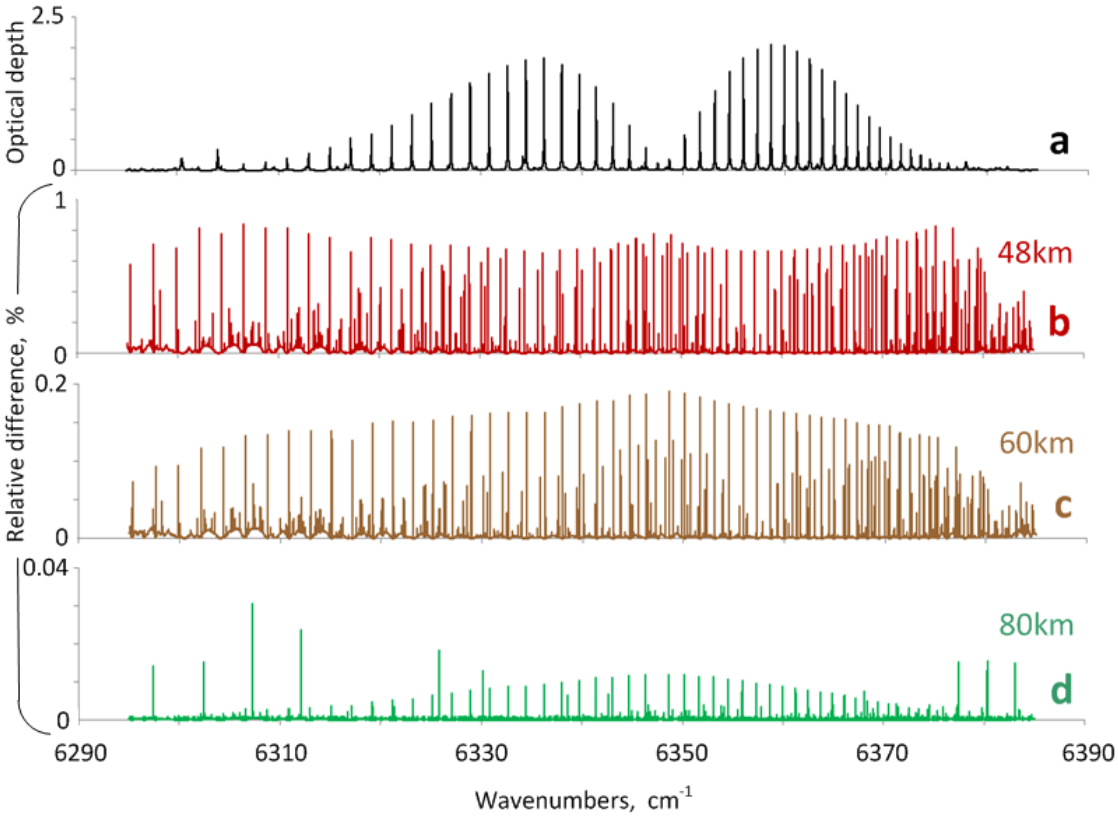

Fig 4 Effect of the vertical path elevation cutoff effect on the accuracy of transmission calculations for the 1.57 micron band of CO_2 (a – Total optical depth spectrum for a 100km altitude calculation, b, c, d – relative differences between the calculations with cutoff altitudes of 48, 60, and 80 km and the 100km (a) spectrum respectively).

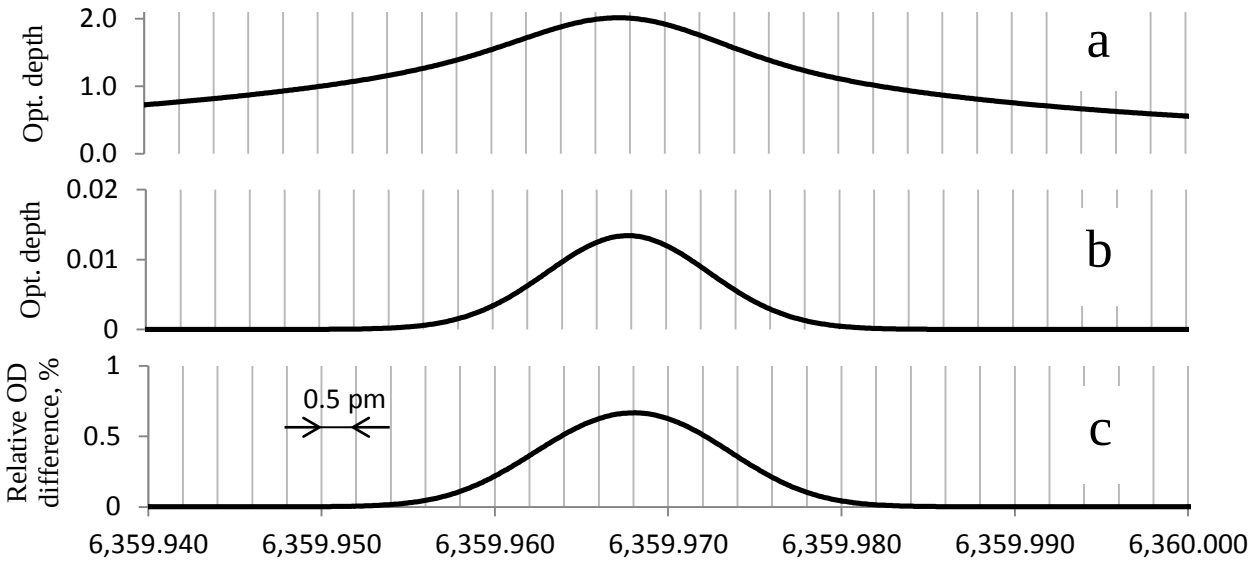

Fig 5 Effect of the vertical path elevation cutoff effect on the accuracy of the transmission calculations for the 6359.9674 cm^{-1} line of CO_2 being investigated by the Goddard group (a – Total optical depth spectrum for a path length of 100km; b, and c – absolute and relative differences between the spectrum in (a) and that calculated with the 48km cutoff altitude respectively).

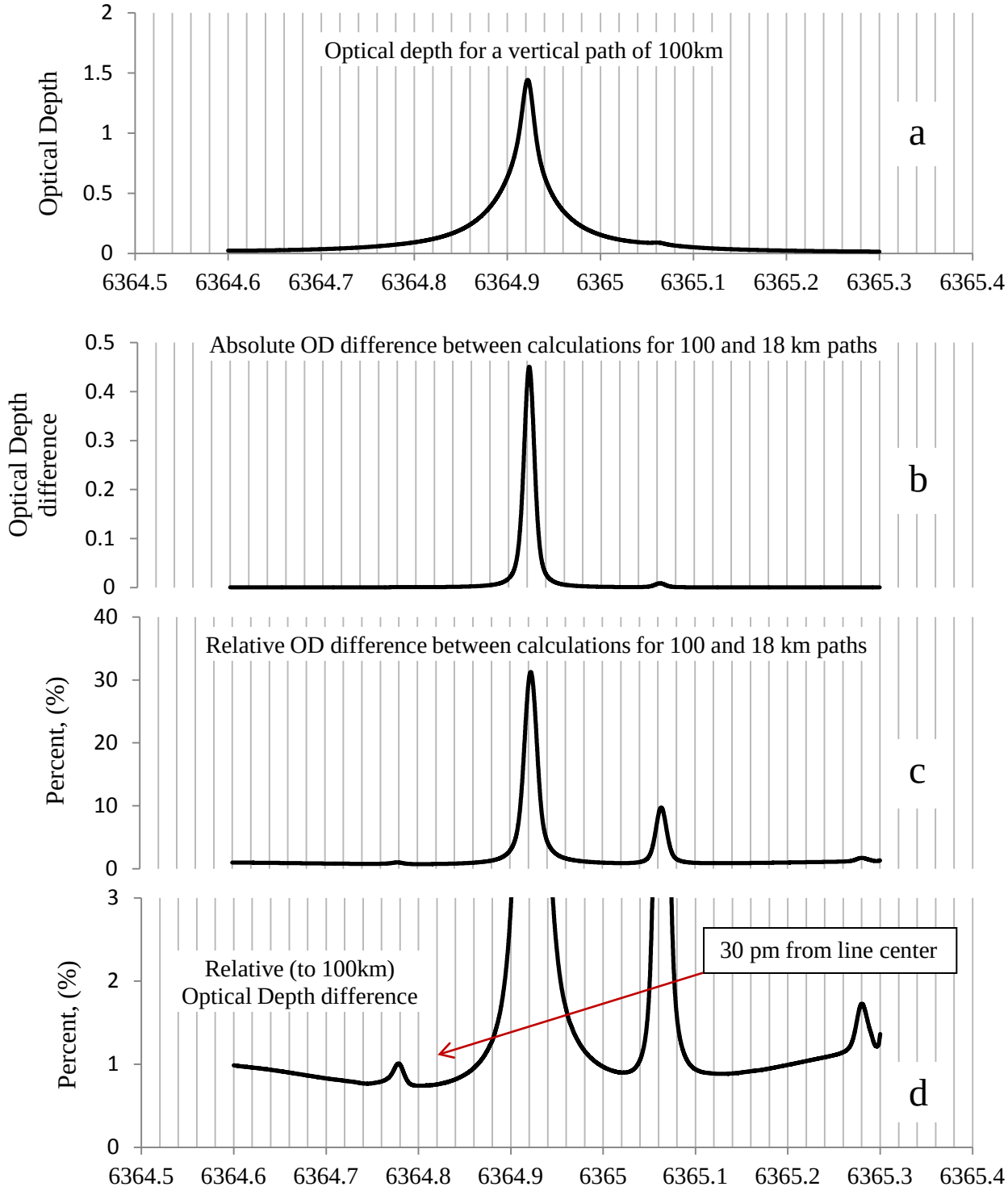

Fig 6 Evaluation of the optical depth differences for transmission calculations with the cutoff altitudes of 100km (standard maximum altitude in the LBLRTM model) and that of 18km corresponding to the Global Hawk measurement altitude. (a – Total optical depth spectrum for an altitude of 100km; b – absolute difference between the optical depths obtained for the calculated altitudes of 100km and 18km; c, and d – relative optical depth differences for the calculations with 100 and 18km altitudes on the vertical scale of 40 and 3 percent respectively).

3.3 Usage of the World Geodetic System (WGS84) standards

To eliminate approximation errors related to the use of the hydrostatic equation for altitude conversions as well as to link the atmospheric models with the surface elevation and other satellite data correctly, all calculations in the framework are referenced to the World Geodetic System (WGS) 84 standard. In particular the values of the acceleration of gravity at sea level and the related radius are calculated using formulas provided below [20].

The WGS 84 acceleration of gravity at sea level ellipsoidal gravity formula:

$$g_0(\varphi) = 9.7803267714 \cdot \frac{1+0.00193185138639 \cdot sin^2\varphi}{(1-0.00669437999013 \cdot sin^2\varphi)^{1/2}} \quad (1)$$

Geocentric radius to the surface of the ellipsoid:

$$R_0(\varphi') = \frac{a(1-e^2)^{1/2}}{(1-e^2 cos^2\varphi')^{1/2}} \quad (2)$$

Radius of curvature in the meridian (R_M):

$$R_M = \frac{a(1-e^2)}{(1-e^2 sin^2\varphi)^{3/2}} \quad (3)$$

Radius of curvature in the prime vertical (R_N):

$$R_N = \frac{a}{(1-e^2 sin^2\varphi)^{1/2}} \quad (4)$$

Relation between the geocentric and geodetic latitudes:

$$\varphi' = \arctan[(1-e^2) \cdot tan(\varphi)] \quad (5)$$

where φ' is the geocentric latitude, φ is the geodetic latitude, a – semimajor axis of the ellipsoid, and e is first eccentricity. In addition to the above WGS 84 standard equations, the earth Geoid altitude corrections from the EGM96 model are applied [21]. The WGS84 standard formulas are further used in the conversions from the pressure levels into altitudes.

3.4 Hydrostatic equation application in atmospheric models

Neglect of such factors as the elliptical shape of the earth, variation of the acceleration of gravity with altitude etc. significantly impact the values of altitude levels in the atmospheric models and consequently the accuracy of the line-by-line calculations. We have estimated the combined error due to these factors to contribute more than 1% (depending on location) into the modeled optical depth uncertainties if unaccounted for.

The error contribution to the acceleration of gravity is estimated as follows [22]:

- Changes of acceleration with altitude (~ 0.3% difference per 10 km)
- Earth elliptical shape (up to ~ 0.7% in sea level g value)
- Effects of centrifugal force on the value of g at varying latitudes (up to ~ 0.3 %)

These errors are passed into the atmospheric transmission modeling through the conversions of pressure levels into altitude in the atmospheric models using the hydrostatic equation:

$$\partial \ln(p) = \frac{g(\varphi,z)}{R_d \cdot T_v} \partial z \tag{6}$$

where ρ is the air density, g – acceleration of gravity, R_d – gas constant for dry air, T_v – virtual temperature, φ is the geodetic latitude. The virtual temperature is calculated as follows:

$$T_v = T \frac{\epsilon + w}{\epsilon \cdot (1+w)} \approx (1 + 0.61 \cdot w) \cdot T \tag{7}$$

where T is the temperature in Kelvin, w is the water vapor mixing ratio in kg of water vapor per kg of dry air, $\epsilon = R_d/R_v$, R_v - gas constant for water vapor. The acceleration of gravity change with altitude may be approximated as follows:

$$g_0(\varphi, z) = \frac{G \cdot M}{(R_0(\varphi)+z)^2} \approx \frac{G \cdot M}{R_0(\varphi)^2} \left[1 - 2\left(\frac{z}{R_0(\varphi)}\right)\right] \tag{8}$$

$$g_0(\varphi) = \frac{G \cdot M}{R_0(\varphi)^2} \tag{9}$$

where G - is the universal gravitational constant, M - mass of the Earth, z – elevation above the earth surface, $R_o(\varphi)$ – radius of the earth as a function of latitude and longitude (Earth geoid radius), z – elevation above the sea level at a given geodetic latitude φ, and $g_0(\varphi)$ is the acceleration of gravity at the ground level $R_o(\varphi)$ which is expressed as follows:

$$R_0(\varphi) = R_{elliptical} + \Delta R_{Geoid} \tag{10}$$

$$R(\varphi) = R_0(\varphi) + z \tag{11}$$

$$g(\varphi, z) = g_0(\varphi, z) - \omega^2 \cdot R(\varphi) \cdot cos^2(\varphi') \tag{12}$$

where $g_0(\varphi, z)$ is the acceleration of gravity value without the centrifugal force component at a given latitude and elevation, $g(\varphi, z)$ – acceleration of gravity corrected for the centrifugal force for a given latitude and elevation, ω – angular velocity of the Earth, $R_{elliptical}$ - geocentric radius to the surface of the ellipsoid, ΔR_{Geoid} – geoid correction value to the $R_{elliptical}$, φ and φ' are the geodetic and geocentric latitude values respectively.

Substituting the above equations for the acceleration of gravity as a function of latitude, and the Earth rotation gravity reduction term into the hydrostatic equation and solving for the altitude, the difference in altitude Δz corresponding to a given pressure difference is expressed as follows:

$$ax^2 + bx + c = 0 \quad ; \quad z_{1,2} = \frac{-b \pm \sqrt{b^2 - 4ac}}{2a} \quad ; \quad \Delta z = z(p_1) - z(p_2) \tag{13}$$

$$a = \frac{g_0}{R_0(\varphi)} + \frac{\omega^2 \cdot cos^2(\varphi\prime)}{2} \quad ; \quad b = -g_0 + \omega^2 \cdot R_0(\varphi) \cdot cos^2(\varphi') \quad ; \quad c = R_d \cdot T_v \cdot \ln(p) \tag{14}$$

where φ' and φ are geocentric and geodetic latitude values respectively corresponding to the same point on the earth surface. When the ASTER global digital elevation model is used, the $R_0(\varphi)$ corresponds to the earth Geoid radius as a function of latitude and longitude (WGS84 value with the EGM96 Geoid correction).

3.5 Surface elevation, and surface reflection

The surface elevation values in our simulation are retrieved from an independent dataset, currently the ASTER-GDEM elevation model [7]. This approach provides higher flexibility in merging different satellite data sources compared to the approaches where the elevation data reported along with one of the surface or atmospheric parameters in satellite data files is used (i.e. CALIPSO data products etc.) The surface elevation data is used in conversions of the MERRA pressure values into the altitude levels as well as to determine the satellite-to-ground path. Since the accuracy of the ASTER dataset varies depending on the surface coordinates, alternative surface elevation datasets or their combinations may be implemented later for increased accuracy.

For the surface reflection data a method previously implemented by Kawa et al. was adopted [13]. The difference in our approach is the use of the 500 meter grid data and the extension of the method to other bands of both CO_2 (1.57 and 2.05 μm band) and O_2 (A-band and 1.26-1.27μm) by using the MODIS BRDF-adjusted reflectance values reported in different spectral channels.

Our current approach does not involve spatial averaging of the ASTER-GDEM surface elevation values or the MODIS reflectance data; instead a point closest to the location coordinates is used in calculations.

3.6 Laser wavelength jitter analysis

The magnitude of the optical depth retrieval error due to the laser wavelength jitter is determined by the slope of the spectral absorption curves. Preliminary estimates of the laser wavelength jitter error contributions for the 1.57 and 2.05 micron bands of CO_2 have been reported by the ESA A-SCOPE group [14, 15].

Our wavelength jitter sensitivity analysis currently uses the output optical depth spectra of the LBLRTM program and provides the capability to analyze both the total optical depth jitter error as well as that as a function of altitude which relies on the layer-by-layer optical depth output of the LBLRTM. The analysis may be performed on either CO_2 or O_2 as well as any other molecule for which transmission calculations may be performed. The current version of LBLRTM supports calculations for 39 line-by-line molecules with additional capabilities of cross-sectional calculations. Such altitude dependent laser wavelength jitter error analysis provides information on the distribution of laser jitter error as a function of altitude which is a useful additional parameter indicating the maximum achievable Optical Depth retrieval accuracy at varying altitude levels for a given laser wavelength instability. For example, Fig. 7 shows the output layer-by-layer optical depth spectrum (a) of the LBLRTM program for a total path of 74 km and 74 equidistant layers and the selected measurement laser line position at 6364.9 cm^{-1} as well as the corresponding distribution of the laser wavelength jitter related error in percent as a function of altitude (b) at the selected central wavelength. Fig. 8 shows the corresponding total laser jitter related optical depth error for a laser stable to within 15MHz as a function of wavenumber.

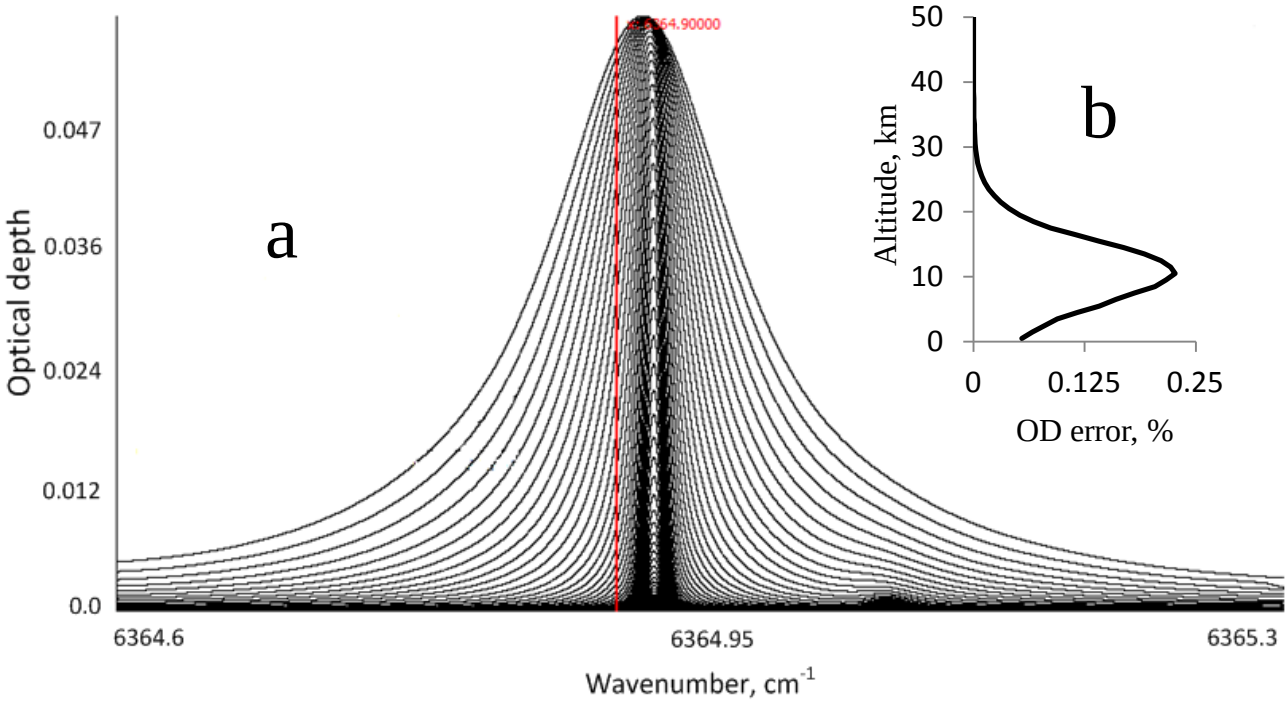

Fig 7 Layer-by-layer line-by-line transmission calculation using LBLRTM and a US standard atmosphere for a vertical path of 74 km and 74 layers (a), and the altitude distribution of the optical depth error induced by the laser wavelength jitter of 15MHz with the laser positioned at 6364.9 cm^{-1} (b) relative to the total optical depth at the selected laser position.

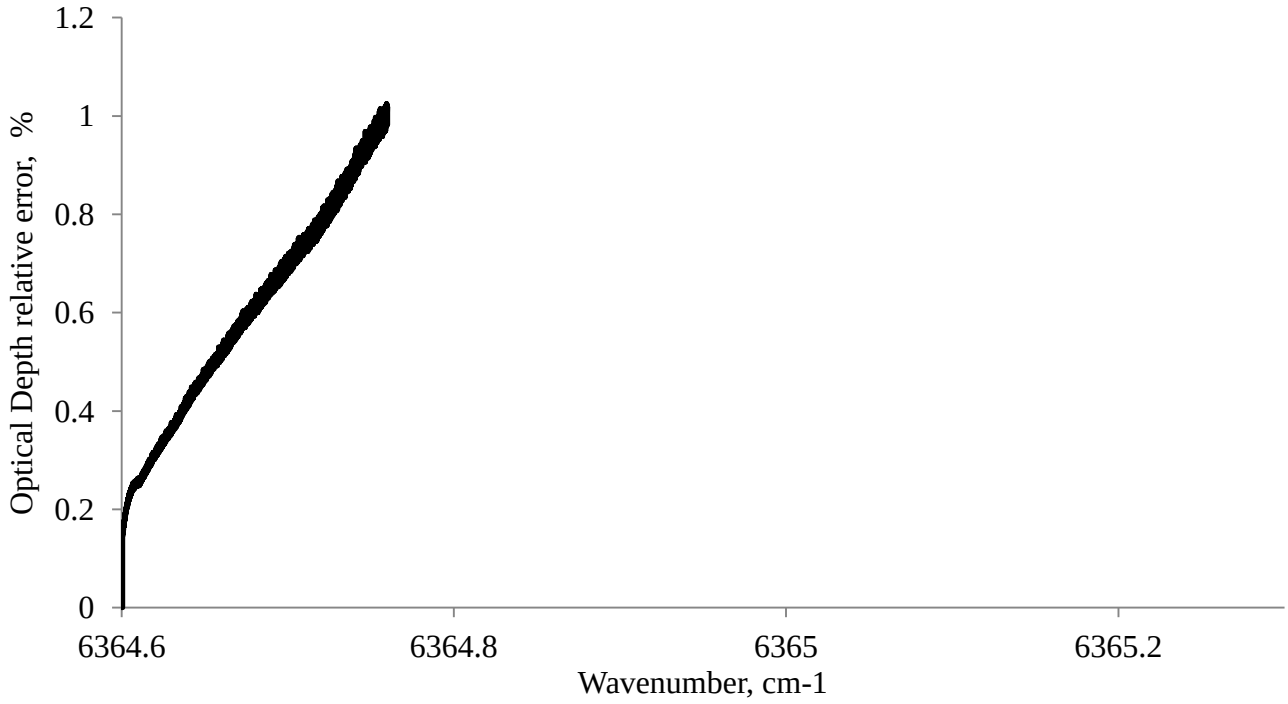

Fig 8 Laser wavlength jitter induced error for a laser with 15MHz wavelength jitter as a function of varying laser position.

3.7 Weighting functions

The weighting function analysis in the framework is currently based on the LBLRTM program to simulate the transmission spectra for various path geometries. Such spectra are analyzed for subsequent selection of the weighting functions by investigating various combinations of on/off line wavelengths.

The weighting function is a measure of altitude dependent absorption for a given molecule expressed as the optical depth per unit of altitude or pressure change and per unit of concentration (such as per 1ppmv) as a function of altitude. The weighting function is typically normalized to unity. For the IPDA approach the optical depth is a differential value between the measurements at the on and off wavelengths as observed at varying altitudes or pressure levels. As such the weighting function for the IPDA measurement approach may be expressed as follows [23]:

$$W(z) = \left.\frac{d\tau(z)}{dz}\right|_{CO2=1\ ppmv} = N_{air}(z) \cdot \Delta\sigma_{CO_2}(z)$$

where *W(z)* is the weighting function, $d\tau$ is the differential optical depth for a chosen pair of on/off wavelengths at a given altitude, $N_{air}(z)$ is the number of all particles in the gas at a given altitude, and $\Delta\sigma_{CO_2}(z)$ is the absorption cross-section of the CO_2 molecule at a given altitude.

Since our approach relies on the use of the external LBLRTM routine, the calculations of the weighting functions are performed by first applying the hydrostatic equation to the input atmospheric models, performing the layer-by-layer LBLRTM program calculations based on the atmospheric models obtained, and then analyzing the layer-by-layer optical depth output spectra for individual molecules (or combined spectra) and selected on/off wavelengths using the input atmospheric models data. Since the weighting functions are expressed per unit concentration of the absorbing gas, the optical depth values obtained in our LBLRTM-based calculation approach for individual altitudes are also adjusted with the corresponding atmospheric model values of CO_2 concentrations for corresponding altitudes. Additional laser wavelength jitter analysis provides extra information on the uncertainties in the total optical depth retrievals and the weighting functions as a function of altitude. This technique is currently being further applied in our studies.

4. THE DATABASE OF MOLECULAR CONCENTRATION PROFILES

Our plans include the expansion of the atmospheric models to additional molecules by using 3-dimentional concentration data from different assimilation sources such as satellite mission measurements by NASA and other agencies. As an example of the feasibility of this approach, the default calculation mode in the frequently used LBLRTM program includes only 7 most abundant molecules in the atmosphere which provides sufficient accuracy for many applications. These molecules include H_2O, CO_2, O_3, N_2O, CO, CH_4, and O_2. The historical 3D atmospheric profile information for some of these molecules (H_2O, CO_2, and O_2) is already available for the last 10 years or longer and is being used in our simulations. In addition, ongoing missions provide data for certain other molecules. An example is the CO molecule and the associated MOPITT mission. Such data usually has the time resolution on the order of 3 to 12 hours with a global latitude and longitude coverage grid of several hundred kilometers. As such it would be beneficial to create a database of 3D mixing ratio profiles for atmospheric gases which would rely on a uniform format such as netCDF or HDF for easy simultaneous usage by line-by-line codes. Our efforts include creation of a database compilation of this kind in support of the modeling framework we developed.

This approach would be a useful alternative to using the US Standard models from 1976 for realistic location and time specific performance predictions for various types of geometries and spectroscopic measurements in the atmosphere.

5. CONCLUSION

A modeling framework for space or airborne lidar sensing applicable to the simulations for ASCENDS and other missions was developed. Our initial calculations indicate a large number of errors resulting from the atmospheric models usage, laser stability and the selection of excitation wavelengths. We are in the process of carrying out more thorough calculations using the framework we developed to better quantify these errors. Comparative studies are under way for the alternative bands of CO_2 (1.57 μm or 2.05 μm) and O_2 (A-band or 1.26-1.27 μm).

The framework does not at present account for the accuracy limitations of the Voigt profile. While the additional error of ~ 0.5% introduced due to the use of the Voigt profile has to be accounted for, other factors such as those related to the correct usage of atmospheric models and the selection of cut-off altitudes introduce a more significant contribution to the overall simulation uncertainty and as such have to be addressed prior to making improvements to the lineshape functions used.

6. ACKNOWLEDGEMENTS

The authors acknowledge the support from the Earth Science Technology Office (ESTO) and the NASA Postdoctoral Program (NPP). The information about the format of the AER LBLRTM spectral output binary TAPE files was obtained through MATLAB exchange from a code posted by Xianglei Huang.

7. REFERENCES

[1] "Active Sensing of CO_2 Emissions over Nights, Days, and Seasons (ASCENDS) Mission", NASA Science Definition and Planning Workshop, July 23-25, 2008, Univ. of Michigan, Ann Arbor, MI, available at http://decadal.gsfc.nasa.gov/documents/12-30-08-ASCENDS_Workshop.pdf

[2] S.A. Clough, M.W. Shephard, E.J. Mlawer, J.S. Delamere, M.J. Iacono, K. Cady-Pereira, S. Boukabara, P.D. Brown, "Atmospheric radiative transfer modeling: a summary of the AER codes", JQSRT, **91**, 233-244, (2005)

[3] L. S. Rothman et al.,"The HITRAN 2008 molecular spectroscopic database", JQSRT, **110**, 533-572, (2009)

[4] L. S. Rothman et al., "The HITRAN molecular database and HAWKS (HITRAN atmospheric Workstation) 1996 edition", JQSRT, 60, 665-710, (1998)

[5] Peters et al, 2007, "An atmospheric perspective on North American carbon dioxide exchange: CarbonTracker", PNAS, **104**, no. 48, 18925-18930, (2007)

[6] Rienecker, M.M., M.J. Suarez, R. Gelaro, R. Todling, J. Bacmeister, E. Liu, M.G. Bosilovich, S.D. Schubert, L. Takacs, G.-K. Kim, S. Bloom, J. Chen, D. Collins, A. Conaty, A. da Silva, et al., **"** MERRA - NASA's Modern-Era Retrospective Analysis for Research and Applications", J. Climate, 24, 3624-3648, 2011, doi: 10.1175/JCLI-D-11-00015.1

[7] NASA Land Processes Distributed Active Archive Center (LP DAAC). ASTER-GDEM is a product of METI and NASA, USGS/Earth Resources Observation and Science (EROS) Center, Sioux Falls, South Dakota. 2001.

[8] Schaaf, C. B., F. Gao, A. H. Strahler, W. Lucht, X. Li, T. Tsang, N. C. Strugnell, X. Zhang, Y. Jin, J.-P. Muller, P. Lewis, M. Barnsley, P. Hobson, M. Disney, G. Roberts, M. Dunderdale, C. Doll, R. d'Entremont, B. Hu, S. Liang, and J. L. Privette, and D. P. Roy, "First Operational BRDF, Albedo and Nadir Reflectance Products from MODIS", Remote Sens. Environ., **83**, 135-148, 2002.

[9] Winker, David M., Mark A. Vaughan, Ali Omar, Yongxiang Hu, Kathleen A. Powell, Zhaoyan Liu, William H. Hunt, Stuart A. Young, "Overview of the CALIPSO Mission and CALIOP Data Processing Algorithms",. J. Atmos. Oceanic Technol., **26**, 2310–2323, (2009), doi: http://dx.doi.org/10.1175/2009JTECHA1281.1

[10] D. Pliutau, and N. S. Prasad, "Development of an Open-source Space or Airborne Multi-wavelength LIDAR Modeling Framework and Accompanying Programs with Application to the ASCENDS Mission," in Lasers, Sources, and Related Photonic Devices, OSA Technical Digest (CD), OSA, 2012, paper LT6B.10.
[11] Denis Pliutau, Narasimha S. Prasad, "Development of an open source LIDAR modeling framework for space or airborne multi-wavelength LIDAR in support of the ASCENDS mission", AGU Fall Meeting 2011, San Francisco, CA
[12] Denis Pliutau, Narasimha S. Prasad, "Improvements of CO2 and O2 Transmission Modeling with Application to the ASCENDS Mission", XVI Coherent Laser Radar Conference (CLRC) 2012, Long Beach, CA, 20-24 June 2012
[13] S. R. Kawa, J. Mao, J. B. Abshire, G. J. Collatz, X. Sun, and C. J. Weaver, "Simulation studies for a space-based CO_2 lidar mission", Tellus B, **62B**, 759-769, (2010)
[14] Jerome Caron, Yannig Durand, "Operating wavelengths optimization for a spaceborne lidar measuring atmospheric CO_2", Appl. Opt. **48**, 5413-5422 (2009).
[15] Jerome Caron, Yannig Durand, Jean-Loup Bezy, Roland Meynart, "Performance modeling for A-SCOPE, a space borne lidar measuring atmospheric CO2", Proc. SPIE, Vol 7479, p. 74790E-1, (2009)
[16] C. Kiemle, M. Quatrevalet, G. Ehret, A. Amediek, A. Fix, and M. Wirth, "Sensitivity studies for a space-based methane lidar mission", Atm. Meas. Tech, Disc., **4**, 3545-3592, (2011)
[17] G. Ehret, C. Kiemle, M. Wirth, A. Amediek, A. Fix, S. Houweling,,"Space-borne remote sensing of CO_2, CH_4, and N_2O by integrated path differential absorption lidar: sensitivity analysis", Appl. Phys. B, **90**, pp. 593-608, (2008)
[18] Robert T. Menzies, and David M. Tratt, "Differential laser absorption spectrometry for global profiling of tropospheric carbon dioxide: selection of optimum sounding frequencies for high-precision measurements", Applied Optics, Vol 42, No. 33, pp. 6569-6577, (2003)
[19] S. R. Kawa, D. J. Erickson III, S. Pawson, and Z. Zhu, J. of Geophys. Res.,"Global CO_2 transport simulations using meteorological data from the NASA data assimilation system", Vol. 109, D18312, (2004)
[20] World Geodetic System 1984 (WGS 84), available at
http://earth-info.nga.mil/GandG/publications/tr8350.2/tr8350.2-a/Chapter%203.pdf
http://earth-info.nga.mil/GandG/publications/tr8350.2/tr8350.2-a/Chapter%204.pdf
[21] F. G. Lemoine, S. C. Kenyon, J. K. Factor, R.G. Trimmer, N. K. Pavlis, D. S. Chinn, C. M. Cox, S. M. Klosko, S. B. Luthcke, M. H. Torrence, Y. M. Wang, R. G. Williamson, E. C. Pavlis, R. H. Rapp and T. R. Olson, "The Development of the Joint NASA GSFC and the National Imagery and Mapping Agency (NIMA) Geopotential Model EGM 96", NASA Goddard Space Flight Center, Greenbelt, Maryland, 20771 USA, July 1998, description available at
http://cddis.nasa.gov/926/egm96/egm96.html
[22] Grant W. Petty "A first course in atmospheric thermodynamics", Sundog Publishing, 2008
[23] Susan Kooi, Jianping Mao, James B. Abshire, Edward V. Browell, Clark J. Weaver, Stephen R. Kawa, "Analysis of Vertical Weighting functions for lidar measurements of atmospheric CO_2 and O_2", **A21D**, 2011 AGU Fall Meeting, San Francisco, CA, 2011.